ORIGINAL ARTICLE

Characterization of the biliary tract by virtual ultrasonography constructed by gadolinium ethoxybenzyl diethylenetriamine pentaacetic acid-enhanced magnetic resonance imaging

Yohei Koizumi · Masashi Hirooka · Hironori Ochi · Yoshio Tokumoto · Megumi Takechi · Atsushi Hiraoka · Yoshio Ikeda · Teru Kumagi · Bunzo Matsuura · Masanori Abe · Yoichi Hiasa

Abstract

Purpose This study aimed at prospectively evaluating bile duct anatomy on ultrasonography and evaluating the safety and utility of radiofrequency ablation (RFA) assisted by virtual ultrasonography from gadolinium ethoxybenzyl diethylenetriamine pentaacetic acid (Gd-EOB-DTPA)-enhanced magnetic resonance imaging (MRI).

Methods The institutional review board approved this study, and patients provided written informed consent prior to entry into the study. Bile duct anatomy was assessed in 201 patients who underwent Gd-EOB-DTPA-enhanced MRI for the evaluation of hepatic tumor. Eighty-one of these patients subsequently underwent RFA assisted by ultrasound imaging. In 23 patients, the tumor was located within 5 mm of the central bile duct, as demonstrated by MRI.

Results Virtual ultrasonography constructed by Gd-EOB-enhanced MRI was able to visualize the common bile duct, left hepatic duct, and right hepatic duct in 96.5, 94.0, and 89.6 % of cases, respectively. The target hepatic tumor nodule and biliary duct could be detected with virtual ultrasonography in all patients, and no severe complications occurred.

Conclusion The running pattern of the bile ducts could be recognized on conventional ultrasound by referencing virtual ultrasonography constructed by Gd-EOB-DTPA-enhanced MRI. RFA assisted by this imaging strategy did not result in bile duct injury.

Keywords Hepatocellular carcinoma · Radiofrequency ablation · Virtual ultrasonography · Gadolinium ethoxybenzyl diethylenetriamine pentaacetic acid · Bile duct

Abbreviations

HCC	Hepatocellular carcinoma
RFA	Radiofrequency ablation
Gd-EOB-DTPA	Gadolinium ethoxybenzyl diethylenetriamine pentaacetic acid
MRI	Magnetic resonance imaging
US	Ultrasound
CT	Computed tomography
PEI	Percutaneous ethanol injection

Y. Koizumi · M. Hirooka · H. Ochi · Y. Tokumoto · Y. Ikeda ·
T. Kumagi · B. Matsuura · M. Abe · Y. Hiasa (✉)
Department of Gastroenterology and Metabology, Ehime
University Graduate School of Medicine, Toon,
Ehime 791-0295, Japan
e-mail: hiasa@m.ehime-u.ac.jp

M. Takechi
Department of Radiology, Ehime University Graduate School
of Medicine, Toon, Ehime 791-0295, Japan

A. Hiraoka
Gastroenterology Center, Ehime Prefectural Central Hospital,
Ehime, Japan

Introduction

Radiofrequency ablation (RFA) is used for potentially curative therapy of hepatocellular carcinoma (HCC) and hepatic metastasis from primary colorectal adenocarcinoma [1–4]. This strategy is associated with low rates of morbidity and mortality and a high level of efficacy [5–7]. Although the incidence of severe complications is low when ablation is performed by an experienced radiologist or hepatologist, severe complications may occur when nodules are in close approximation to

critical structures and organs [6, 8–10]. In particular, tumors that are close to the hepatic hilum may be unsuitable for percutaneous RFA because of the risk of injuring adjacent bile ducts [10]. Indeed, the heat generated by RFA can cause bile ductal stenosis with dilation of the upper bile duct or abscess formation [11, 12]. Some investigators have suggested that a minimal distance of 1.5–2 cm from the ablated area to the proximal intrahepatic bile duct is necessary to avoid bile duct heat injury [13–16]. However, it is difficult to identify intrahepatic bile ducts on conventional ultrasound (US) imaging, and this modality is, therefore, unable to appropriately determine a site for puncture that is not in close approximation to the bile duct. Instead, the electrode is typically inserted away from the portal vein, because the portal vein is visible and because the bile duct usually runs close to this vein.

Gadolinium ethoxybenzyl diethylenetriamine pentaacetic acid (Gd-EOB-DTPA) is a hepatocyte-specific contrast agent that has a prolonged T1-shortening effect on the liver parenchyma [17–19]. After injection, rapid and specific hepatocyte uptake with biliary excretion occurs at approximately 50 % of the injected dose. Magnetic resonance (MR) cholangiography can be potentially enhanced by this contrast medium. Using the virtual ultrasonographic image [20, 21] constructed by Gd-EOB-DTPA-enhanced magnetic resonance imaging (MRI), it may be possible to derive the location of the intrahepatic bile duct on the conventional US image.

Therefore, the goal of this study was to prospectively evaluate the bile duct anatomy on ultrasonography and to evaluate the safety and utility of RFA assisted by virtual ultrasonography from Gd-EOB-DTPA-enhanced MRI.

Patients and methods

Patients

The ethics committee of our institution approved all study protocols. Written informed consent to participate in the study was obtained prior to enrollment in accordance with the principles of the Declaration of Helsinki. A total of 201 patients (148 men, 53 women, mean age 68.0 ± 10.0 years, age range 35–89 years) underwent Gd-EOB-DTPA-enhanced MRI for the evaluation of hepatic tumor at the Department of Gastroenterology and Metabology, Ehime University Graduate School of Medicine, Ehime, Japan, between October 2009 and May 2013. First, bile duct anatomy was evaluated in these patients (Fig. 1). Eighty-one (58 men, 23 women, mean age 69.0 ± 8.7 years, age range 48–84 years) of these patients then underwent RFA or percutaneous ethanol injection (PEI) guided by ultrasound images. All patients underwent abdominal ultrasonography, contrast-enhanced computed tomography (CT), and Gd-EOB-DTPA-enhanced MRI before treatment. A consecutive entry design was used, and 23 patients with HCC tumors closer than 5 mm to the central bile duct at the hepatic hilum (demonstrated by CT and MRI images) were enrolled. All patients underwent abdominal ultrasonography or contrast-enhanced CT every 3 months after RFA to evaluate the treated lesion.

Gd-EOB-DTPA-enhanced MRI

MR imaging was performed with superconductive 3.0-Tesla (3-T) and 1.5-T imaging units (Achieve, Phillips Healthcare, Best, The Netherlands). All systems were equipped with high-performance gradient systems. For all

Fig. 1 Flow chart of trial participants
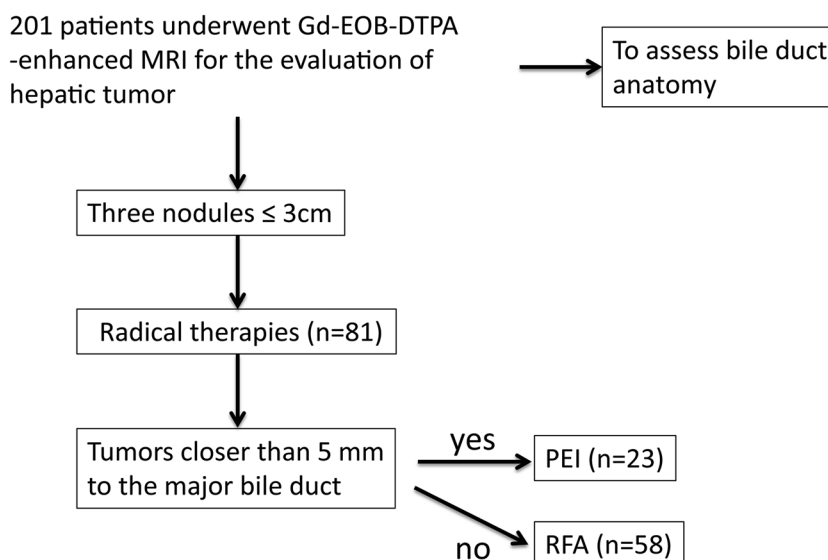
patients, an MR-compatible power injector (Sonic Shot GX, Nemoto Kyorindo, Tokyo, Japan) was used to deliver a bolus injection of Gd-EOB-DTPA at 3 ml/s at a dose of 25 μmol/kg body weight (0.1 ml/kg) via a 22-gauge intravenous catheter placed in an antecubital vein. A 30-ml saline flush was administered at 3 ml/s after gadoxetate injection. Unenhanced MRI was obtained using a T1-weighted gradient echo (GRE) sequence (dual echoes; in-phase and out-of-phase). For dynamic study, the arterial phase and delayed phase were obtained. Scan timing of dynamic MRI was determined using a bolus tracking method triggered by pulmonary arterial enhancement. Triple-arterial phase images were acquired with T1 high-resolution volumetric examination (THRIVE). The first arterial phase was started at an average of 9 s after the pulmonary arterial enhancement. Total scan time for triple-arterial dynamic MRI was 15 s. Delayed phase images were obtained 60 and 120 s after the injection of Gd-EOB-DTPA. The hepatobiliary phase images were obtained 20 min after the injection of Gd-EOB-DTPA in all cases. MR parameters of the hepatobiliary phase T1-weighted GRE for the Gd-EOB-DTPA-enhanced images were as follows for the 1.5-T MR system: TR, 3.9 ms; TE, 1.9 ms; flip angle, 9°; SENSE factor, 1.8 (anteroposterior direction); slice thickness, 2.5 mm; matrix, 255×256; and field of view, 350 mm. Parameters for the 3.0-T MR system were as follows: TR, 3.5 ms; TE, 1.69 ms; flip angle, 10°; SENSE factor, 1.8 (anteroposterior direction); slice thickness, 2.4 mm; matrix, 256×512; and field of view, 350 mm.

Imaging and cholangiography

First, the adequacy of biliary duct depiction was evaluated (Fig. 2) by assessing the (1) common bile duct (CBD), (2) left or right hepatic duct (LHD or RHD), (3) right anterior sectorial duct (RASD), right posterior sectorial duct (RPSD), left medial sectorial duct (LMSD), or left lateral sectorial duct (LLSD), and (4) branch of caudate process, Spiegel lobe, and paracaval portion. Bile duct anatomy variants were then assessed as previously described [22]. The biliary configurations in the right liver lobe were classified as types A–J and are described herein as types Ar–Jr, respectively: in configuration type Ar, the RPSD (B6–B7 junction) joins the RASD (B5–B8 junction) with a supraportal course (classic pattern); in type Br, the RPSD joins the LHD with a supraportal course; type Cr is a triple confluence of the RASD, RPSD, and LHD; in type Dr, the RPSD joins the RASD with an infraportal course; in type Er, the RPSD joins the common hepatic duct with an infraportal course; and types Fr–Jr are other, rare biliary variations. The confluence patterns in the left liver lobe were mainly classified as types A–C, which are described herein as types Al–Cl, respectively: in confluence pattern type Al, the common trunk of B2 and B3 joins B4; type Bl is a triple confluence of B2, B3, and B4; in type Cl, B2 drains into the common trunk of B3 and B4; and the other types include a pattern in which two ducts from one segment take two different drainage paths, Fr, and other patterns. The running courses of the lateral-segmental ducts of the left lobe were classified as supraportal type or
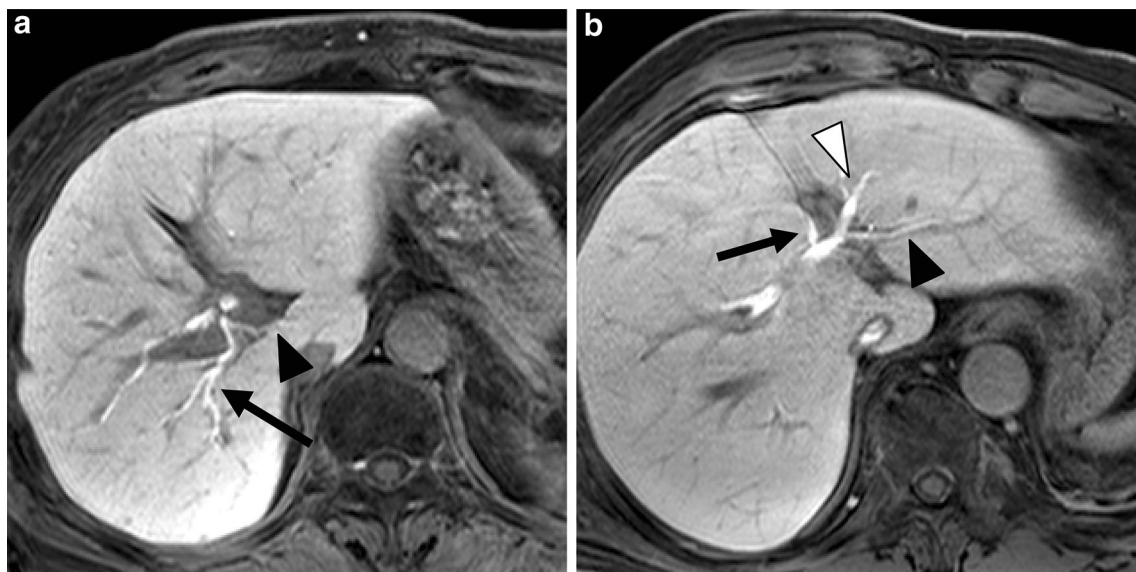

Fig. 2 MR cholangiography using Gd-EOB-DTPA. Axial Gd-EOB-DTPA-enhanced T1-weighted images obtained 20 min after injection are shown. **a** Intrahepatic bile ducts in the right lobe are shown. The right posterior sectorial duct (*black arrow*) runs cranially to the right anterior portal vein. **b** The left major branch of B2 (*black arrowhead*) and B3 (*white arrow head*) joins B4 (*black arrow*). The course of the lateral segmental duct is supraportal

infraportal type. Cholangiography imaging was evaluated by two hepatologists (Y.K. and M.H., with 10 and 16 years of experience, respectively).

Radiofrequency ablation

Radiofrequency ablation was performed using a Cool-Tip RF system (Radionics, Burlington, MA, USA), which is a 480-kHz alternative current generator that can produce a maximum power of 180 W through a 17-gauge monopolar cooled-tip needle electrode. All radiofrequency ablations were performed percutaneously by one of three experienced hepatologists (Y.K., M.H., H.O., with 7–16 years of experience) in sonographically guided interventional procedures and radiofrequency ablation. Before treatment, 15 mg of pentazocine hydrochloride and 25 mg of hydroxyzine hydrochloride were administered intramuscularly. Local anesthesia was induced by 5 mL of 1 % lidocaine. Blood pressure, respiration, pulse, and electrocardiograms were continuously monitored. A ground pad was affixed to the thighs of the patients. Tissue impedance and power output status was monitored throughout the procedure. Prior to puncture, the three-dimensional (3D) anatomical relationships between the tumor and the intrahepatic bile duct were sufficiently examined, and the distances were measured on a real-time virtual sonography (RVS) system. Ablation was completed when breakdown occurred a third time. For tumors in contact with the intrahepatic bile duct, treatment with PEI was recommended. After ablation, the therapeutic effect was assessed based on the hyperechoic rim. The hyperechoic rim on US represents the necrotic area [23].

Real-time virtual sonography

B-mode sonography, including the use of a RVS system (Preirus; Hitachi Medical Systems, Tokyo, Japan) during RFA, was performed with a 3.5-MHz curved array transducer. The RVS system consists of a transmitter and magnetic sensor that detects the position of the sonographic probe. RVS provides the same cross-sectional multiplanar reconstruction (MPR) images as ultrasound (US) images on the same monitor screen in real time, using DICOM volume data. Prior to RFA treatment, DICOM volume data from CT or MRI were loaded on the RVS apparatus. We synchronized B-mode ultrasound images with MPR images according to timing of inspiration. This imaging technique displayed a real-time synchronized multiplanar MR image (the hepatobiliary phase images) in precisely the same slice of the US plane in 81 patients.

Statistical analysis

Data are expressed as mean $\pm$ standard deviation (SD). A value of $p < 0.05$ was considered to indicate statistical significance. Interobserver agreement regarding the evaluation of the bile duct images was evaluated by calculation of kappa coefficients. Univariate logistic regression was performed with the Wald test. All data were analyzed with JMP software (version 8; SAS Institute Japan, Tokyo, Japan).

Results

Patients

The characteristics of the 201 patients (148 men, 53 women; mean age, 68.0 $\pm$ 10.0 years) are shown in Table 1. Child-Pugh class A disease was present in 171 patients, Child-Pugh class B disease was present in 23 patients, and Child-Pugh class C disease was present in seven patients with cirrhosis. Thirty-three patients were positive for hepatitis B surface antigen, 99 patients were positive for hepatitis C virus, and 69 patients were negative for both hepatitis B surface antigen and hepatitis C virus. Further, 81 patients with HCC were treated with percutaneous RFA.

Variant of bile duct anatomy

Visualization of the biliary duct by Gd-EOB-enhanced MRI (Figs. 2, 3) is shown in Table 2. The common bile duct, LHD, and RHD were visualized in 96.5, 94.0, and 89.6 % of cases, respectively. RASD (74.1 %) and RPSD (80.1 %) were also depicted on virtual ultrasonography, and LLSD and LMSD were visualized in 74.6 and 67.7 %

Table 1 Characteristics of the patients

Sex	
Female	53
Male	148
Age, years (age range)	68.0 $\pm$ 10.0 (35–89)
Child-Pugh grade	
A	171
B	23
C	7
Etiology	
HBs antigen positive	33
HCV antibody positive	99
NBNC	69
Estimated GFR (ml/min/1.73 m^2)	76.7 $\pm$ 19.6 (36.0–161.3)
MR imaging	
3.0-T	158
1.5-T	43

HBs hepatitis B surface, *HCV* hepatitis C virus, *NBNC* non-B non-C hepatitis

Fig. 3 Virtual ultrasonography using Gd-EOB-DTPA-enhanced MRI. **a** Intrahepatic bile duct image generated by virtual ultrasonography. **b** Conventional ultrasonographic images are shown. The location of the intrahepatic bile duct is not clear
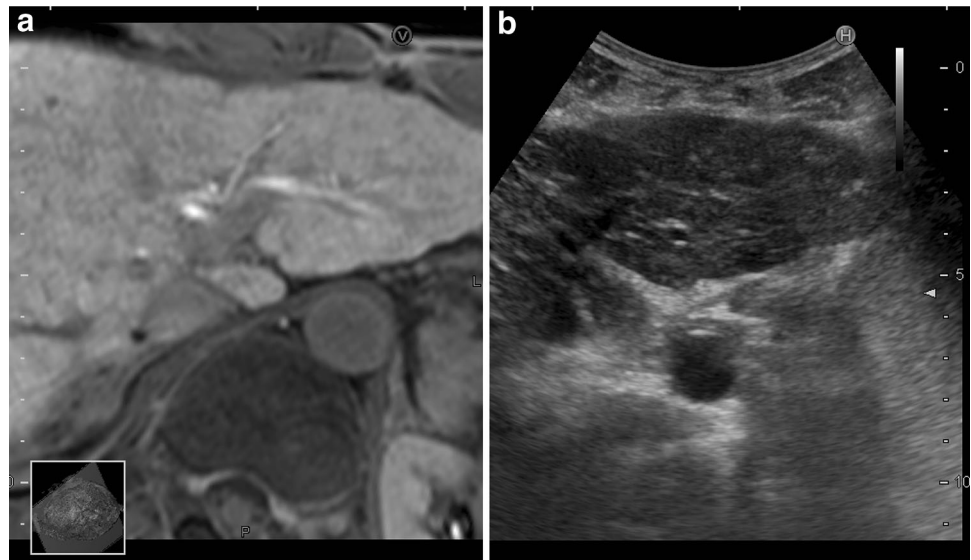

Table 2 Visualization of the bile ducts

	Visible/invisible (%)	n (%)
Common bile duct	194/7 (96.5)	
Major right branch	189/12 (94.0)	
Anterior segmental branch	149/52 (74.1)	
B8	97/104 (48.2)	
B5	95/106 (47.3)	
Posterior segmental branch	161/40 (80.1)	Ar 146 (73.1)
B7	89/112 (44.3)	Br 4 (1.9)
B6	84/117 (41.8)	Cr 9 (4.5)
		Dr 1 (0.5)
		Er 1 (0.5)
Major left branch	180/21 (89.6)	
Lateral segmental branch	150/51 (74.6)	Al 126 (62.7)
B2	120/81 (59.7)	Bl 5 (2.5)
B3	113/88 (56.2)	Cl 11 (5.5)
Medial segmental branch	136/65 (67.7)	Dl 2 (1.0)
B4a	60/141 (29.9)	
B4b	120/81 (59.7)	
Caudate process	12/189 (6.0)	
Paracaval portion	21/180 (10.4)	
Spiegel lobe	41/160 (20.4)	

Table 3 Factors affecting biliary duct depiction (logistic regression model)

	Odds ratio (95 % CI)	P value
Anterior segmental branch		
Age	1.42 (1.00–2.01)	0.046
Sex	1.23 (0.79–1.95)	0.366
Creatinine	0.75 (0.11–4.42)	0.759
3 T vs. 1.5 T	0.71 (0.48–1.07)	0.098
Child-Pugh A vs. non A	0.42 (0.27–0.63)	<0.0001
Posterior segmental branch		
Age	1.69 (1.01–1.22)	0.008
Sex	1.11 (0.71–1.77)	0.366
Creatinine	1.90 (0.21–13.78)	0.543
3 T vs. 1.5 T	0.58 (0.37–0.90)	0.0158
Child-Pugh A vs. non A	0.42 (0.27–0.63)	<0.0001
Lateral segmental branch		
Age	1.75 (1.20–2.59)	0.004
Sex	0.89 (0.56–1.43)	0.643
Creatinine	2.12 (0.27–13.93)	0.543
3 T vs. 1.5 T	0.40 (0.26–0.60)	<0.0001
Child-Pugh A vs. non A	37 (0.23–0.58)	<0.0001
Medial segmental branch		
Age	1.43 (1.02–2.03)	0.040
Sex	0.86 (0.56–1.31)	0.643
Creatinine	1.65 (0.27–9.02)	0.543
3 T vs. 1.5 T	0.39 (0.26–0.58)	<0.0001
Child-Pugh A vs. non A	0.44 (0.28–0.68)	<0.0001

of cases, respectively. The right biliary configuration types were Ar in 73.1 %, Br in 1.9 %, Cr in 4.5 %, Dr in 0.5 %, and Er in 0.5 % of the subjects. The left biliary configuration types were Al in 62.7 %, Bl in 2.5 %, Cl in 5.5 %, and Dl in 1 % of the subjects. Factors affecting biliary duct depiction included age, MRI imaging (3-T or 1.5-T), and Child-Pugh score (Table 3). The kappa value for visible or invisible was excellent ($\kappa = 0.951 \pm 0.043$ [mean $\pm$ standard error (SE)]).

Real-time virtual sonography

Virtual ultrasonography using Gd-EOB-DTPA MRI is shown in Fig. 3. Recognition of the intrahepatic bile duct

Fig. 4 Major pattern of right lobe bile duct variance evaluated by virtual ultrasonography. Bile duct branching patterns depicted by virtual ultrasonography are shown. **a** The major right bile duct runs on the major right portal vein. **b** The branch of the bile duct runs parallel to the portal vein in the anterior segment. **c** The right posterior sectorial duct (*black arrowhead*) runs perpendicular to the right anterior portal vein
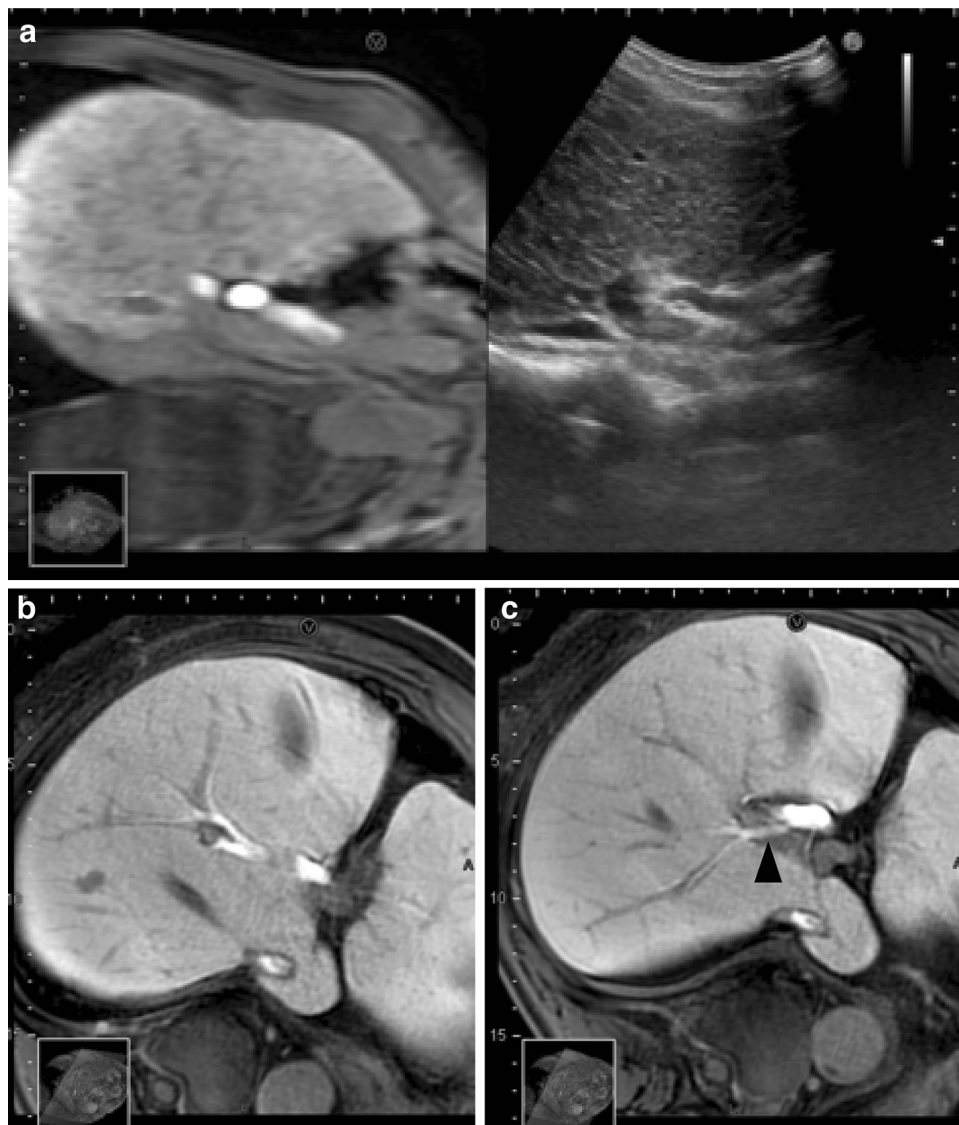
was difficult when using conventional ultrasonography, but was successful when using virtual ultrasonography (Fig. 4).

On conventional US imaging, the common bile duct, LHD, and RHD were visualized in 94.8, 43.1, and 34.5 % of cases, respectively, while the RASD, RPSD, LLSD, and LMSD were depicted in 3.4, 5.1, 6.9, and 1.7 % of cases, respectively. Third-order biliary branches could not be visualized. Further, common bile duct visualization was possible in all cases when using the virtual ultrasound. The LHD and RHD were visualized in 92.6 and 97.5 % of cases, respectively, while the RASD, RPSD, LLSD, and LMSD were depicted in 80.2, 79.0, 72.8, and 67.9 % of cases, respectively. Visualization of third-order biliary branches (with the exception of B4a) was successful in 40.7–59.3 % of cases. The major patterns of the right lobe

bile duct anatomy, as evaluated by virtual ultrasonography, are shown in Fig. 4.

Radiofrequency ablation

The target HCC nodule and biliary duct were detected with RVS in all patients. Twenty-three nodules were located in close approximation to the major bile duct and were treated with ethanol injection therapy. Ablation was safely performed in the other 58 patients. After RFA, mild pain and fever were noted, but no severe complications occurred. Contrast-enhanced CT performed 1 week after RFA showed complete local tumor ablation in all patients. The median follow-up period after RFA was 11 months (range, 7–17 months). Dilation of the intrahepatic bile duct was not observed on CT obtained 3 months after RFA. No local
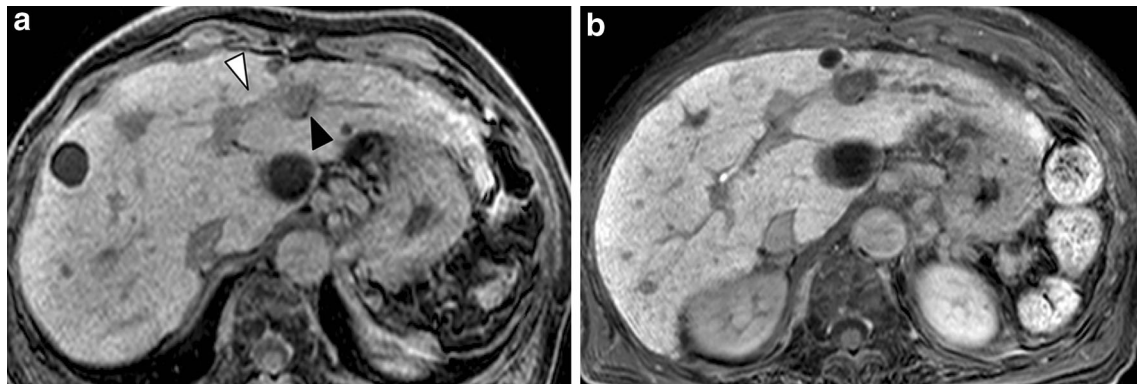
Fig. 5 A case of bile duct heat injury after radiofrequency ablation. **a** The target tumor (*black arrow*) was in close approximation to the left major branch of B3 (*white arrow*). **b** After ablation of this nodule, heat injury to B3 occurred, with subsequent dilatation of this branch

Fig. 6 A case without bile duct heat injury after radiofrequency ablation. **a** CTAP before ablation is shown. The target nodule is depicted as a perfusion defect (*black arrow*). **b** Though this target nodule is in close approximation to the major portal branch (P3), this nodule is on the opposite side across the branch of the bile duct (B3) (duct marked with *white arrow* in *left panel*). The *right panel* shows the conventional ultrasonographic images of the same region. **c** Contrast-enhanced CT after ablation is shown. Heat injury did not occur

recurrence was observed in any patients. RFA was technically feasible, and local tumor control was achieved in all patients.

Discussion

In the present study, biliary tract anatomy could be depicted in sonographic imaging combined with virtual ultrasonography constructed by Gd-EOB-DTPA-enhanced MRI. Moreover, RFA was performed empirically for patients with HCC close to Glisson's capsule after assessing the configuration of the biliary tract. The target HCC nodule and biliary duct could be detected with RVS in all patients, and no severe complications occurred.

There are two obstacles to detection of the bile duct on US images. First, the bile duct is often obscured on US, even more so in patients with cirrhosis in whom intrahepatic echogenicity is often diminished. The narrow diameter and histological structure (columnar epithelium) of the bile duct contribute to this difficulty in detection via US. Second, the biliary anatomy may vary between individuals. This problem has already been discussed in the case of hepatic surgical treatment, i.e., to reduce the surgical risk, accurate estimation of the vascular and biliary configuration is needed [24]. Similarly, knowledge of biliary anatomy, especially with regard to the anterior branch and posterior branch, is critical when performing RFA to reduce the risk of heat injury to the bile ducts (Fig. 5). Indeed, Stippel et al. [25] described four cases of bile duct complications (9.5 %), including three bile duct strictures and one bile duct stricture with biloma among 42 patients who were treated with liver resection and RFA. Various methods have been proposed as means of avoiding bile duct injury, including prophylactic placement of a biliary stent [26] and intraductal cooling of the bile duct during RFA [27]. Although these methods may prevent thermal injury to the central bile ducts, it is an invasive procedure. The present study demonstrated that the configuration of the bile ducts can be characterized using RVS. Thus, we were able to prevent bile duct injury even if we did not recognize biliary dissection accurately (Fig. 6).

The RVS system using Gd-EOB-DTPA-enhanced MRI has several limitations. First, this modality cannot be employed in patients with allergies to Gd-EOB-DTPA or in patients who have contraindications to MRI examination, such as an implanted cardiac pacemaker. Second, the synchronized image from the RVS system does not completely match the actual imaging slice from ultrasonography. Thus, careful evaluation with imaging is necessary after RFA assisted by the RVS system. Third, we used the RVS system in all RFA cases. Therefore,

comparison between the RVS system and the standard method for RFA was not possible. Fourth, this study had no gold standard and therefore does not represent a controlled trial.

In conclusion, the running pattern of the bile ducts could be recognized on conventional ultrasound by referencing virtual ultrasonography constructed by Gd-EOB-DTPA-enhanced MRI. RFA assisted by this imaging strategy did not result in bile duct injury.

Conflict of interest There are no financial or other relations that could lead to a conflict of interest.

Human rights statements and informed consent All procedures followed were in accordance with the ethical standards of the responsible committee on human experimentation (institutional and national) and with the Helsinki Declaration of 1975, as revised in 2008 (5). Informed consent was obtained from all patients for being included in the study.

References

1. Rossi S, Di Stasi M, Buscarini E, et al. Percutaneous RF interstitial thermal ablation in the treatment of hepatic cancer. AJR Am J Roentgenol. 1996;167:759–68.
2. Allgaier HP, Deibert P, Zuber I, et al. Percutaneous radiofrequency interstitial thermal ablation of small hepatocellular carcinoma. Lancet. 1999;353:1676–7.
3. Curley SA, Izzo F, Delrio P, et al. Radiofrequency ablation of unresectable primary and metastatic hepatic malignancies: results in 123 patients. Ann Surg. 1999;230:1–8.
4. Livraghi T, Goldberg SN, Lazzaroni S, et al. Small hepatocellular carcinoma: treatment with radio-frequency ablation versus ethanol injection. Radiology. 1999;210:655–61.
5. Tateishi R, Shiina S, Teratani T. Percutaneous radiofrequency ablation for hepatocellular carcinoma. An analysis of 1000 cases. Cancer. 2005;103:1201–9.
6. Livraghi T, Solbiati L, Meloni MF, et al. Treatment of focal liver tumors with percutaneous radio-frequency ablation: complications encountered in a multicenter study. Radiology. 2003;226:441–51.
7. de Baere T, Risse O, Kuoch V, et al. Adverse events during radiofrequency treatment of 582 hepatic tumors. AJR Am J Roentgenol. 2003;181:695–700.
8. Mulier S, Mulier P, Ni Y, et al. Complications of radiofrequency coagulation of liver tumours. Br J Surg. 2002;89:1206–22.
9. Chopra S, Dodd GD III, Chanin MP, et al. Radiofrequency ablation of hepatic tumors adjacent to the gallbladder: feasibility and safety. AJR Am J Roentgenol. 2003;180:697–701.
10. McGhana JP, Dodd GD 3rd. Radiofrequency ablation of the liver: current status. Am J Gastroenterol. 2001;176:3–16.

11. Bilchik AJ, Rose DM, Allegra DP, et al. Radiofrequency ablation: a minimally invasive technique with multiple applications. Cancer J Sci Am. 1999;5:356–61.

12. Nordlinger B, Rougier P. Nonsurgical methods for liver metastases including cryotherapy, radiofrequency ablation, and infusional treatment: what's new in 2001? Curr Opin Oncol. 2002;14:420–3.

13. De Baere T, Elias D, Dromain C, et al. Radiofrequency ablation of 100 hepatic metastases with a mean follow-up of more than 1 year. AJR Am J Roentgenol. 2000;175:1619–25.

14. Dodd GD, Soulen MC, Kane RA, et al. Minimally invasive treatment of malignant hepatic tumors: at the threshold of a major breakthrough. Radiographics. 2000;20:9–27.

15. Pearson AS, Izzo F, Fleming D, et al. Intraoperative radiofrequency ablation or cryoablation for hepatic malignancies. Am J Surg. 1999;178:592–9.

16. Elias D, De Baere T, Mutillo I, et al. Intraoperative use of radiofrequency treatment allows an increase in the rate of curative liver resection. J Surg Oncol. 1998;67:190–1.

17. Hamm B, Staks T, Mühler A, et al. Phase I clinical evaluation of Gd-EOB-DTPA as a hepatobiliary MR contrast agent: safety, pharmacokinetics, and MR imaging. Radiology. 1995;195:785–92.

18. Reimer P, Rummeny EJ, Shamsi K, et al. Phase II clinical evaluation of Gd-EOB-DTPA: dose, safety aspects, and pulse sequence. Radiology. 1996;199:177–83.

19. Bluemke DA, Sahani D, Amendola M, et al. Efficacy and safety of MR imaging with liver-specific contrast agent: U.S. multicenter phase III study. Radiology. 2005;237:89–98.

20. Kudo M. New sonographic techniques for the diagnosis and treatment of hepatocellular carcinoma. Hepatol Res. 2007;37:S193–9.

21. Minami Y, Chung H, Kudo M, et al. Radiofrequency ablation of hepatocellular carcinoma: value of virtual CT sonography with magnetic navigation. AJR Am J Roentgenol. 2008;190:W335–41.

22. Kitami M, Takase K, Murakami G, et al. Types and frequencies of biliary tract variations associated with a major portal venous anatomy: analysis with multi-detector row CT cholangiography. Radiology. 2006;238:156–66.

23. Uehara T, Hirooka M, Kisaka Y, et al. Usefulness of the hyperechoic rim for assessing the therapeutic efficacy of radiofrequency ablation in hepatocellular carcinoma patients. Hepatol Res. 2009;39:954–62.

24. Saba L, Mallarini G. Anatomic variations of arterial liver vascularization: an analysis by using MDCTA. Surg Radiol Anat. 2011;33:559–68.

25. Stippel DL, Tox U, Gossmann A, et al. Successful treatment of radiofrequency-induced biliary lesions by interventional endoscopic retrograde cholangiography (ERC). Surg Endosc. 2003;17:1965–70.

26. Wood TF, Rose M, Chung M, et al. Radiofrequency ablation of 231 unresectable hepatic tumors: indications, limitations, and complications. Ann Surg Oncol. 2000;7:593–600.

27. Ohnishi T, Yasuda I, Nishigaki Y, et al. Intraductal chilled saline perfusion to prevent bile duct injury during percutaneous radiofrequency ablation for hepatocellular carcinoma. J Gastroenterol Hepatol. 2008;23:410–5.